Thermal conductivity, electron transport, and magnetic properties of single-crystal $Ca_3Co_2O_6$

J.-G. Cheng, J.-S. Zhou,* and J. B. Goodenough
Texas Materials Institute, University of Texas at Austin, Austin, Texas 78712, USA
(Received 7 January 2009; revised manuscript received 30 March 2009; published 12 May 2009)

A recent neutron-diffraction study on the magnetic insulator $Ca_3Co_2O_6$ shows that spins in the *c*-axis chains of alternating Co1 octahedral and Co2 trigonal-prismatic face-sharing $CoO_{6/2}$ sites are ordered below T_N with a long-wavelength modulation instead of a simple ferromagnetic chain as thought previously. Frustrated antiferromagnetic interchain interactions compete with ferromagnetic intrachain coupling to invalidate an Ising model despite a strong spin-orbit coupling $\lambda \mathbf{L}\cdot\mathbf{S}$ on the Co2 ions. We have carried out thermal conductivity, electron transport, and magnetic measurements on single-crystal $Ca_3Co_2O_6$ in order to characterize this complicated magnetic system. An anisotropic thermal-conductivity component superimposed at high temperatures on an isotropic phonon component is consistent with an exchange-interaction-mediated heat transfer. This observation is incompatible with an Ising model. The ferromagnetic intrachain interactions are argued to reflect a one-dimensional itinerant-electron band that is split by the *c*-axis translational symmetry and the on-site intra-atomic Hund exchange interaction with a localized $S=3/2$ spin on the Co2 ions.

DOI: 10.1103/PhysRevB.79.184414 PACS number(s): 75.30.Et, 71.70.Ej

I. INTRODUCTION

The magnetic insulator $Ca_3Co_2O_6$ has attracted considerable attention since successive steps in the magnetization $M(H_\parallel)$ curve for H parallel to the *c* axis were reported at $T < T_N \approx 24$ K.[1] Corresponding to a large jump in $M(H_\parallel)$, the dielectric constant ε also exhibits a sharp anomaly.[2] As shown in Fig. 1, the $Ca_3Co_2O_6$ structure consists of infinite chains parallel to the *c* axis of alternate Co1 octahedra and Co2 trigonal-prismatic $CoO_{6/2}$ sites sharing faces; these chains projected onto the *ab* plane form a close-packed array. The Ca^{2+} ions are located between the chains.[3] The intrachain Co1-Co2 separation is ~2.6 Å; the interchain Co separation is ~5.2 Å. NMR measurement[4] has confirmed that both the Co1 and the Co2 are trivalent. Refinement of neutron powder diffraction[5] has given average magnetic moments of $0.08\mu_B$ on Co1 and $3.00\mu_B$ on Co2. These observation would correspond to a low-spin $(S=0)t^6e^0$ configuration on the octahedral Co1 and a high-spin $(S=2)[(x^2-y^2)\pm ixy)]^3(3z^2-r^2)^1(yz\pm izx)^2$ configuration on the trigonal-prismatic Co2. Spin-orbit coupling splits the minority-spin $[(x^2-y^2)\pm 2xy)]$, which has a magnetic quantum number $m=2$, to introduce a strong uniaxial magnetic easy-magnetization axis along the *c* axis *z* direction. X-ray magnetic circular dichroism has verified a large orbital magnetic moment of $1.7\mu_B$ on the Co2 at 20 K.[6] The strong spin-orbit $\lambda \mathbf{L}\cdot\mathbf{S}$ coupling led Wu *et al.*[7] to conclude an Ising model is applicable with ferromagnetic Co1-Co2 interactions along the chains in what was thought to be a contradiction of the superexchange rules. With an Ising model for the spins, it was proposed that the steps in the $M(H_\parallel)$ curve correspond to a successive flipping of the spins of near-neighbor chains from antiferromagnetic to ferromagnetic alignment.[8]

This picture has recently been challenged by a neutron-diffraction study on a single-crystal sample.[9] Instead of ferromagnetic spin ordering along the chain, a helical exchange pathway gives rise to a long-wavelength magnetic modulation along the *c* axis. This new finding calls into question the Ising model and the explanation of the steps in the $M(H_\parallel)$ curve. Although the helical exchange pathway does not give a specific magnetization $M(H_\perp)$ with a magnetic field within the *ab* plane, the Ising model predicts an extremely small, paramagnetic $M(H_\perp)$ below T_N. However, no measurement of $M(H_\perp)$ on a $Ca_3Co_2O_6$ crystal has yet been reported as far as we know.

In a magnetic insulator, heat can be transferred by spin-spin exchange interactions as well as by lattice vibrations. Exchange-interaction-mediated (EIM) heat transfer in a quasi-one-dimensional spin system is enhanced in the direction of strong spin-spin coupling or may even be ballistic in the case of $S=1/2$ as has been demonstrated, for example, in Sr_2CuO_3,[10] $SrCuO_2$,[11] and $Sr_{14}Cu_{24}O_{41}$.[12] It has been predicted and shown for the Haldane chain compounds Y_2BaNiO_5 (Ref. 13) and $AgVP_2S_6$ (Ref. 14) with $S=1$ that the enhancement is smaller but remains visible for an $S=1$ system. The EIM heat transfer occurs in the paramagnetic phase at a temperature above the maximum of the phonon-mediated heat transfer. The EIM heat transfer would be negligible in an Ising-spin chain system.[15] Therefore, whether an EIM heat transfer exists in the spin-chain system $Ca_3Co_2O_6$ is critical to test the validity of an Ising model. Reported in this paper, we have carried out a thorough study of thermal conductivity, electron transport, and magnetic properties on a single crystal of $Ca_3Co_2O_6$ in order to find out whether the Ising model is applicable given a relatively strong intrachain ferromagnetic coupling and a strong spin-orbit $\lambda \mathbf{L}\cdot\mathbf{S}$ coupling in the chains. A plausible EIM enhancement of the thermal conductivity has been observed in a $Ca_3Co_2O_6$ crystal at higher temperatures. Moreover, we argue that the ferromagnetic intrachain coupling is due to an indirect exchange interaction between band electrons along the *c* axis and localized spins on the Co2 ions.

II. EXPERIMENTAL DETAILS

Single crystals of $Ca_3Co_2O_6$ were grown by the flux method. In the first step, single-phase, polycrystalline $Ca_3Co_4O_9$ was obtained by calcining a mixture of $CaCO_3$

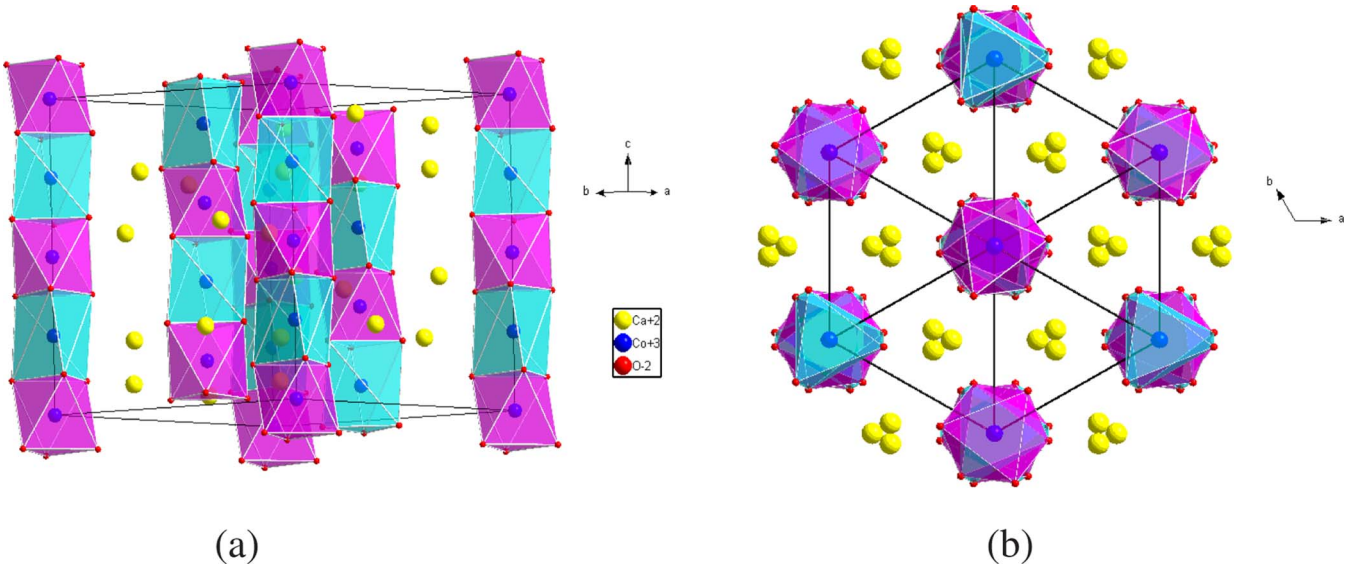

FIG. 1. (Color online) The crystal structure of $Ca_3Co_2O_6$.

and Co_3O_4 in air at 900 °C for 4 days with several intermediate grindings. A mixture of $Ca_3Co_4O_9$ and K_2CO_3 (flux) in a weight ratio of 1:7 was loaded into an aluminum crucible and soaked at 920 °C for 10 h; the crucible was slowly cooled at a rate of 1 °C/h to 820 °C before finally being cooled down to room temperature at a rate of 180 °C/h. The grown crystals were collected by dissolving the solidified charge in deionized water. Phase purity was examined with powder x-ray diffraction (XRD) on pulverized crystals at room temperature with a Philips X'pert diffractometer in the 2θ range 15–100° with steps of 0.02° and a dwell time of 10 s. The observed powder XRD pattern shown in Fig. 2 was refined with the Rietveld method by using the FULLPROF program.[16] The refinement confirms that the as-grown crystals are single phase with the rhombohedral structure (space group $R\bar{3}c$). The structural parameters displayed in Fig. 2 are in good agreement with the values reported in the literature.[3,5] Energy dispersive spectroscopy was carried out on several crystals; the cation ratio is very close to Ca:Co =3:2 with no trace of potassium. A large positive Seebeck coefficient $S \approx 430$ μV/K at room temperature in Fig. 3(a) indicates that the content of Co^{4+} is below 0.7%. Moreover, the temperature dependence of S indicates that $Ca_3Co_2O_6$ is a nearly intrinsic insulator. Figure 3(b) shows the temperature dependence of the resistivity $\rho_{\|}$ along the chain direction and $\rho_{\perp}$ perpendicular to the chains. Although $\rho_{\|}$ is lower than $\rho_{\perp}$ by about two orders of magnitude, the activation energies $\Delta_{\perp}=0.051$ eV and $\Delta_{\|}=0.047$ eV obtained by fitting $\rho(T)$ with a formula of hopping conduction $\rho \sim \exp(T^{-1/2})$ are very close. Thermal conductivity was measured between 8 and 350 K by a steady-state method with a systematic error of up to 15% due to uncertainty in measurement of the sample size and the distance between the thermal couples. A four-probe method was used to measure the resistivity. The magnetization was measured in a superconducting quantum interference device (SQUID) magnetometer (Quantum Design). As shown in the scanning electron microscopy (SEM) photograph of Fig. 2, a typical crystal of $Ca_3Co_2O_6$ has a needle shape about $0.2 \times 0.2 \times 1.5$ mm^3 with the longest dimension coinciding with the c axis of the hexagonal cell. Some larger crystals were also found in the crucible, but they normally consisted of stacking of several small crystals as checked with a microscope. We have selected hexagonal-shaped bars of single-domain crystals from several crystal growths for thermal-conductivity $\kappa(T)$ measurements. Due to the bar shape of a crystal, the measurement along the direction perpendicular to the c axis was made on a crystal that has about 0.5 mm length along the heat-flow direction. The small dimension introduces an even larger uncertainty in the absolute value of $\kappa_{\perp}$. However, the temperature dependence of $\kappa_{\perp}$ remains reliable.

III. RESULTS AND DISCUSSION

A. Thermal conductivity

The thermal conductivity $\kappa(T)$ of single-crystal $Ca_3Co_2O_6$ along directions parallel ($\kappa_{\|}$) and perpendicular ($\kappa_{\perp}$) to the

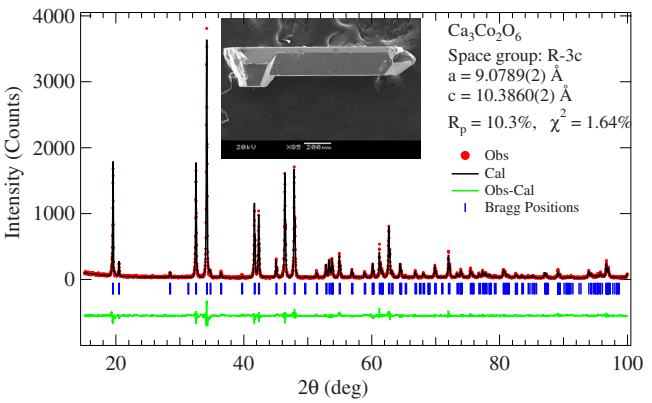

FIG. 2. (Color online) The powder x-ray diffraction of $Ca_3Co_2O_6$ at room temperature and parameters of the Rietveld refinement. The inset displays an SEM photograph of a $Ca_3Co_2O_6$ single crystal.

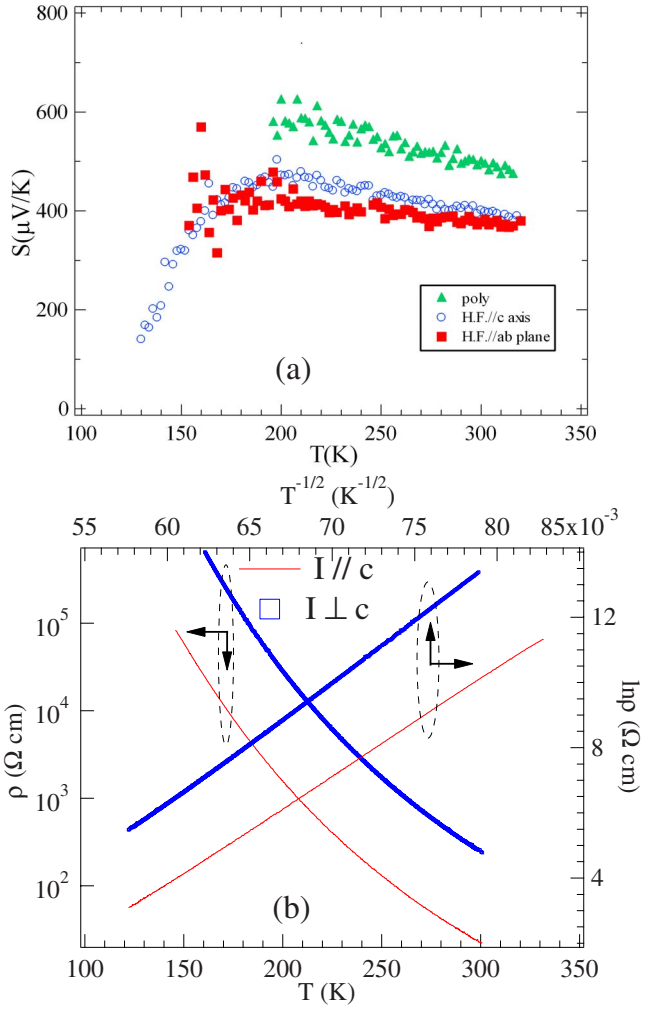

FIG. 3. (Color online) Temperature dependences of (a) thermoelectric power and (b) resistivity of $Ca_3Co_2O_6$.

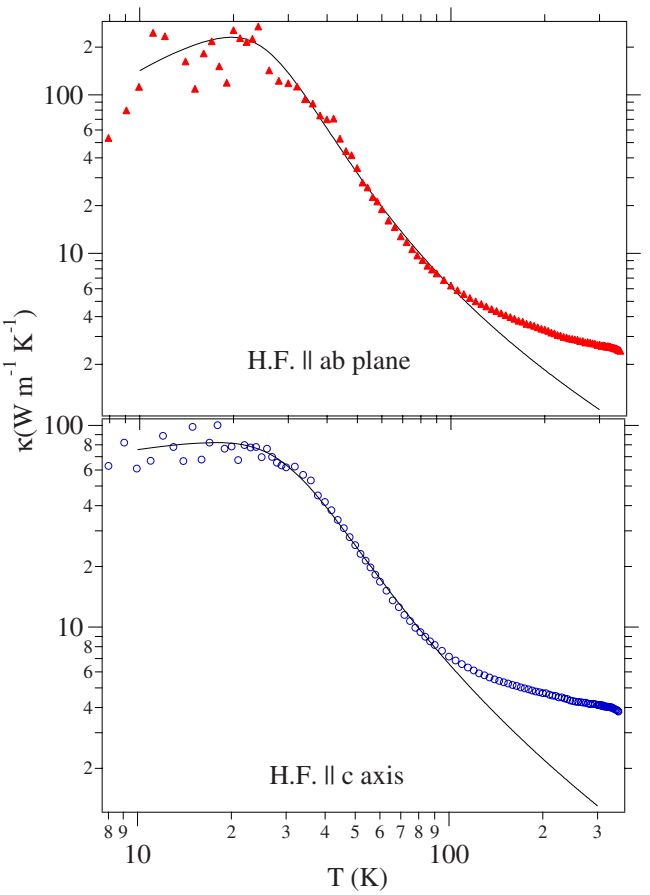

FIG. 4. (Color online) Temperature dependence of thermal conductivity κ with heat flow along the c axis and within ab plane in a $Ca_3Co_2O_6$ single crystal. Lines in the curves are the fitting results with the standard Debye formula for phonon thermal conductivity.

chains are displayed in Fig. 4. Along both directions, κ falls into the range of the best phonon thermal conductivity in oxides at low temperatures. The thermal gradient at these temperatures is too small to be picked up accurately by the differential thermal couple used in our setup. Relatively noisy data do not permit to extract precisely the highest magnitude of thermal conductivity in a $Ca_3Co_2O_6$ crystal and whether there is an anomaly in the curve κ versus T at $T_N \approx 24$ K. Like regular phonon thermal conduction, κ decreases steeply as temperature increases. In order to distinguish whether EIM heat transfer plays a role in the $\kappa(T)$ of $Ca_3Co_2O_6$, we must subtract from κ the phonon contribution.

The phonon contribution to thermal conductivity $\kappa_{\rm ph}(T)$ can be described with the Debye model as follows:[17]

$$\kappa_{\rm ph}(T) = \left(\frac{k_B}{2\pi^2 v}\right)\left(\frac{k_B}{\hbar}\right)^3 T^3 \int_0^{\theta_D/T} \frac{x^4 e^x}{(e^x-1)^2}\tau(\omega,T)dx, \quad (1)$$

where $x=\hbar\omega/k_BT$, v is the average sound velocity, θ_D is the Debye temperature, and $\tau(\omega,T)$ is the relaxation time of a phonon, which can be expressed as

$$\tau^{-1} = v/L + A\omega^4 + B\omega^3 T \exp(-\Theta_D/bT). \quad (2)$$

The first term in Eq. (2) is related to phonon scattering at the sample's boundary, the second is at defects, and the third is phonon-phonon scattering. The $\kappa \sim 1/T$ law is a good approximation of the Debye model at $T \geq \Theta_D$. Since $Ca_3Co_2O_6$ has a relatively high Debye temperature $\Theta_D \approx 390$ K and the measurement of κ is subject to the correction due to thermal-radiation loss above room temperature, the $1/T$ law does not provide a guide for phonon conduction in this crystal. Moreover, the measured temperature dependence of κ is significantly weaker than regular phonon conduction at $150 < T < 300$ K. Therefore, we have performed a fitting with the Debye formula at $T < 100$ K. As shown in Fig. 4, the Debye model fits reasonably well both $\kappa_{\parallel}$ and $\kappa_{\perp}$ in this temperature range, and the fitting parameters listed in Table I are comparable to those for typical phonon conduction.[11–13] At $T > 100$ K, both $\kappa_{\parallel}$ and $\kappa_{\perp}$ show a clear deviation from the phonon conduction. An extra contribution along all directions on top of the phonon conduction has also been observed in other spin-chain systems such as $Sr_{14-x}Ca_xCu_{24}O_{41}$,[12] Sr_2CuO_3,[10] $SrCuO_2$,[11] Y_2BaNiO_5,[13] and $(La,Eu)_{2-x}Sr_xCuO_4$.[18] A common character of this enhancement to $\kappa(T)$ is that it increases with increasing doped-

TABLE I. Parameters of the fitting of $\kappa(T)$ to Eq. (1).

	c axis	ab plane
$L(10^{-4}$ m)	44	1.2
$A(10^{-42}$ s^3)	4.6	0.2
$B(10^{-31}$ K^{-1} S^2)	56.7	68.7
b	3.2	2.8

charge-carrier density. The origin of the deviation has been widely attributed to either the resonant scattering between phonons and magnetic impurities or the contribution from optical phonons. In comparison with other undoped spin-chain systems, the deviation from a phonon conduction is more pronounced in our $Ca_3Co_2O_6$ crystal. Moreover, the clearly anisotropic deviation suggests that an EIM heat transfer contributes along the direction of the spin chains. The EIM heat transfer, however, is relatively weak in our $Ca_3Co_2O_6$ crystal so that the double-shoulder feature in $\kappa(T)$ along the direction of the spin chain that is found in other spin-chain systems[10–13] is not clear here. The presence of an EIM heat transfer indicates that $Ca_3Co_2O_6$ is not an Ising spin system. Moreover, our magnetization measurement with magnetic field perpendicular to the direction of the chains shows an interesting feature which indicates that the spin-spin coupling is not as simple as in an Ising system.

B. Magnetization

Figure 5 shows the magnetic susceptibility χ^{-1} of $Ca_3Co_2O_6$ with H parallel and perpendicular to chains. The $\chi(T)$ of the paramagnetic phase is highly anisotropic. Neither $\chi_\parallel$ nor $\chi_\perp$ follows a Curie-Weiss (CW) law. The data in the literature[19] have only shown $\chi_\parallel$ and $\chi_\perp$ down to 50 K. Our data in a broader range of temperature reveal more detailed

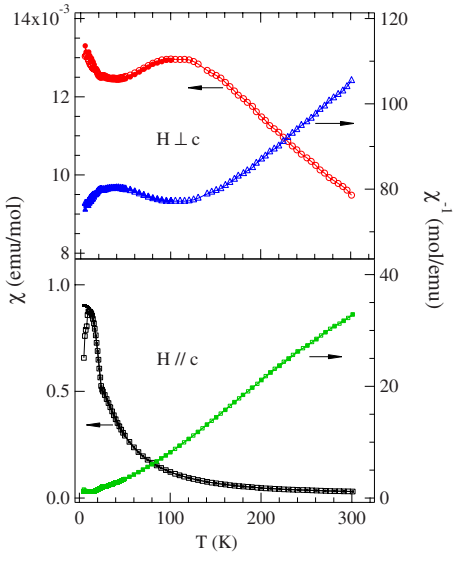

FIG. 5. (Color online) Temperature dependence of the anisotropic inverse magnetic susceptibility of $Ca_3Co_2O_6$ single crystal. The magnetic field $H=5$ T was used in $\chi_\perp$ and $H=1$ T in $\chi_\parallel$.

features of $\chi_\parallel$ and $\chi_\perp$ at T_N and in the spin-ordered phase. Our initial measurements look similar to that in the literature[19] at $T>50$ K. However, after we took a scan of the magnetization at 10 K versus the rocking angle between the magnetic field and the perpendicular direction of the c axis of the crystal, the $\chi_\perp$ at a rocking angle where $M(10$ K) becomes minimum shows a more pronounced maximum near 100 K. By including the spin-orbit $\lambda\mathbf{L}\cdot\mathbf{S}$ coupling, but no spin-spin interaction, Parkin and Friend[20] interpreted the anisotropic $\chi(T)$ of compounds where the orbital angular momentum is not quenched. While Hardy *et al.*[19] claimed that they can fit their anisotropic $\chi(T)$ data at $T>110$ K for $\chi_\perp$ and at $T>50$ K for $\chi_\parallel$ with the model by Parkin and Friend,[20] these fittings turned out to be unreliable for our data in Fig. 5. An entire fit of $\chi(T)$ in the paramagnetic phase appears to require a Hamiltonian that includes exchange interactions and the spin-orbit coupling as put forward by Drillon *et al.*[21] in interpreting $\chi(T)$ in the $9R$ phase of $BaRuO_3$. Nevertheless, we have confirmed three important features in the magnetic susceptibility of $Ca_3Co_2O_6$ with strong spin-orbit $\lambda\mathbf{L}\cdot\mathbf{S}$ coupling: (1) a μ_{eff} significantly larger than the spin-only value, (2) a changing slope of $\chi^{-1}(T)$ that cannot be fit with a CW law, and (3) a highly anisotropic $\chi(T)$. Moreover, we have found two features that are not compatible with the Ising model: (1) $\chi_\perp$ increases at $T<T_N$ and (2) field-cooled $\chi_\parallel$ and zero-field-cooled $\chi_\parallel$ split at $T<T_N$.

The magnetization $M(H_\parallel)$ at $T<T_N$ exhibits a steplike behavior as shown in Fig. 6(a). The dramatic increase in magnetization occurs as $H_\parallel$ increases from zero and also at $H\approx3.6$ T. Smaller steps in $M(H_\parallel)$ are also visible at $H\approx1.2$ and 2.4 T. $M(H_\parallel)$ exhibits a hysterisis loop at the magnetic field where M jumps. In $Ca_3Co_2O_6$, ferromagnetically coupled spin chains are coupled antiferromagnetically to one another. However, a triangular configuration of spin chains results in frustration of the antiferromagnetic interchain interactions. Such frustration leads to many degenerate metastable states.[1,8] A small magnetic field parallel to the spin chains can trigger a switch from one to another. An $M_{\text{sat}}\approx4.8\mu_B$ at $H_\parallel>3.6$ T in the single-crystal sample remained unchanged up to $H=40$ T in a polycrystalline sample,[22] which indicates the Co2 spins are perfectly lined up in the magnetic-field direction. It should also be noticed that the spins are nearly ferromagnetically aligned under $H_\parallel=5$ T at $T=25$ K$>T_N$. The spin ordering at $T<T_N$ introduces plateaus and steps in the $M(H_\parallel)$ curve. The question is whether an entire spin chain flips under the magnetic field as expected from an Ising model or a small portion of the spin chain becomes unlocked under the magnetic field in the long-wavelength magnetic modulation observed by neutron diffraction. We turn to measurements of $M(H_\perp)$ in order to address this issue.

An Ising model[7] for $Ca_3Co_2O_6$ prohibits any possibility that either the spin or the orbital moment has a component in the x-y plane. According to this model, the magnetization $M(H_\perp)$ should be extremely small and linear at all temperatures. As the spin degree of freedom in the x-y plane is eliminated below T_N, the $M(H_\perp)$ at $T<T_N$ may become even lower than that at $T>T_N$. A measurement with a magnetic field perfectly perpendicular to the c axis turned to be not easy. As mentioned in the measurement of $\chi_\perp$, we have first

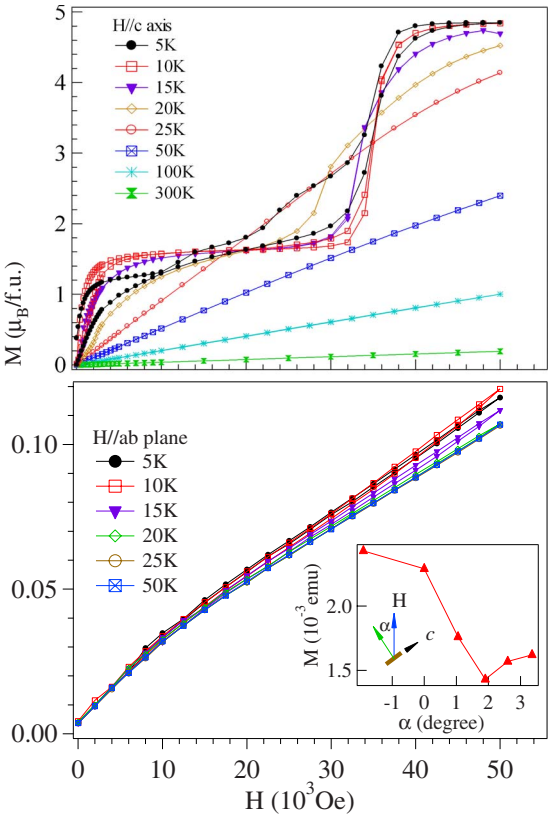

FIG. 6. (Color online) The magnetization at different temperatures of a $Ca_3Co_2O_6$ single crystal with the magnetic field (a) parallel to the c axis and (b) perpendicular to the c axis. Inset is the rocking angle dependence of the magnetization at $T=10$ K and $H=5$ T for the crystal used in $M(H_\perp)$.

taken a scan of the magnetization at 10 K as a function of the rocking angle and all the other magnetization measurements were performed at a rocking angle, where the $M(H_\perp)$ is minimum. Even with this procedure, we found that results are sample-dependent. Samples showing a significantly curved $M(H_\perp)$ with a clear loop may have some parasitic grains with different orientations from the bulk. Figure 6(b) shows $M(H_\perp)$ at different temperatures and the rocking angle dependence of $M_{10\ \mathrm{K}}(5\ \mathrm{T})$ for a crystal exhibiting the smallest loop of $M(H_\perp)$ below T_N. First of all, a slightly curved M-H at about $H=1$ T appears from the device for scanning the rocking angle since it also shows in the $M(H)$ at $T>T_N$. All $M(H)$ curves at $T=20-50$ K overlap with each other. The increase in $M(H_\perp=5\ \mathrm{T})$ at $T<T_N$ is obvious. Although we cannot rule out decisively the possibility that the increase is caused by a small misalignment within 1° of the rocking angle, the nearly temperature-independent $M(H_\perp)$ at $T>T_N$ perhaps due to the strong spin-orbit $\lambda\mathbf{L}\cdot\mathbf{S}$ coupling is sharply different from the $M(H_\parallel)$, which is temperature dependent. Therefore, the increase in $M(H_\perp)$ at $T<T_N$ suggests that spins cant toward the magnetic field direction in the x-y plane, which is consistent with a spiral-spin structure operative in the helical exchange pathway. Although there is no remnant magnetization at $H=0$, a clear hysteresis loop develops between the magnetic field scanning up and scanning down in magnetic field. Since the interchain

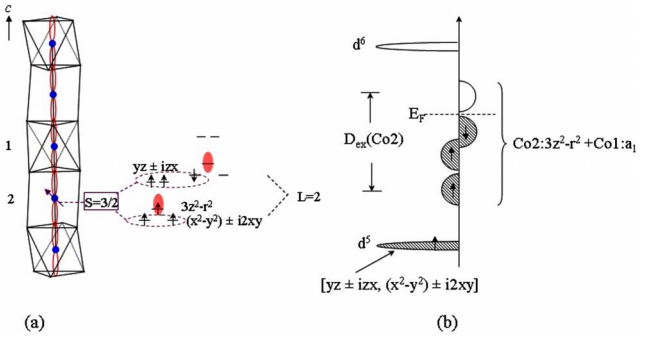

FIG. 7. (Color online) Cartoon of (a) the point-charge model of one-electron energies on Co2 and of (b) localized configuration d^5 on Co2 with itinerant states split by intra-atomic exchange D_{ex}, which concentrates the spin density on the Co2 atoms and by the translational symmetry.

couplings are frustrated, glassy behavior is expected; and we indeed found a magnetization $M(H_\perp)$ relaxation over 30 min after a magnetic field $H_\perp=5$ T was applied. The hysteresis loop observed appears to be caused by the spin relaxation.

An $M(H_\parallel=5\ \mathrm{T})\approx 4.8\mu_B/\mathrm{f.u.}$, which is much larger than $M(H_\perp=5\ \mathrm{T})$, at $T<T_N$, confirms that the Co2-Co2 spin-spin interactions along a chain are ferromagnetic. However, a low-spin ($S=0$) configuration on the octahedral-site Co1 would require an antiferromagnetic spin-spin interaction between half-filled $(3z^2-r^2)$ orbitals on the Co2 according to the rules for the sign of the superexchange interactions. Wu *et al.*[7] justified this apparent discrepancy by making a local spin-density approximation+Hubbard U-band-structure calculation in which holes are introduced into oxygen atoms to give a moment of $0.07\mu_B$ on a Co1 site. Since covalent bonding transfers spin to the ligands in any superexchange model but are normally spin paired through an $S=0$ complex, we offer an alternative and more general justification for ferromagnetic Co2-Co2 intrachain interactions. The 2.6 Å intrachain Co1-Co2 separation is short enough for the formation of an itinerant-electron $(3z^2-r^2)$ one-dimensional (1D) band.[23] As illustrated in Fig. 7, the triginal component of the octahedral Co1 site splits the t^6 configuration into $e_\pi^4 a_1^2$, where the $a_1=(3z^2-r^2)$ overlaps the $(3z^2-r^2)$ orbitals on Co2 to give a $(3z^2-r^2)$ band that is $\frac{3}{4}$ filled. The intrachain ferromagnetic coupling is likely due to the indirect exchange interaction between a 1D band electron along the c axis and localized spins on $[(x^2-y^2)\pm i2xy]$ and $(yz\pm izx)$ orbitals, which contribute a total spin $S=\frac{3}{2}$. However, the indirect exchange interaction here should be distinguished from the regular one since no Fermi surface exists in this magnetic insulator. This 1D band electron picture is also needed to be verified by experiments such as angle-resolved photoemission.

The neutron-diffraction data[9] suggested that spins remain colinear along the c axis with antiferromagnetic interfaces at a much longer and incommensurate periodicity relative to the lattice. On crossing these antiferromagnetic interfaces, the c-axis magnetization goes to zero. Given a constant spin $S=2$ at a Co2 site, we are left with two options to piece together a whole picture of the ordered spin configuration: (a) a spiral-spin structure having a colinear spin in the

middle of a ferromagnetic domain with spins turned into the direction perpendicular to the c axis at an antiferromagnetic interface and (b) a paramagnetic phase and a ferromagnetic phase placed alternatively along the c axis. The first option is more likely since it is compatible with the helical exchange pathway in the structure. Moreover, although the ratio $|J_\perp/J_\parallel|$ of the magnetic-exchange parameters has not been determined in $Ca_3Co_2O_6$, the intrachain and interchain Co2-Co2 bond lengths are very close, which signals that the ratio $|J_\perp/J_\parallel|$ is not too small for a helical spin configuration. A spiral-spin configuration below T_N has been found in the rare-earth $Tm_{1-x}Er_x$ alloys[24] which have the $J_\perp$ component competitive with $J_\parallel$. On the other hand, a relatively large ratio $|J_\parallel/J_\perp|$ is needed to enhance an EIM heat transfer. Whether the enhancement above 100 K of $\kappa(T)$, which is most obvious along the chain direction, is due to an EIM heat transfer or is solely due to excited states associated with strong $\lambda\mathbf{L}\cdot\mathbf{S}$ coupling remains to be determined.

IV. CONCLUSION

Our measurements of the transport properties, thermal conductivity, and magnetic properties of single-crystal $Ca_3Co_2O_6$ characterize further this interesting magnetic insulator containing c-axis chains of alternating octahedral and trigonal-prismatic $CoO_{6/2}$ sites sharing common faces. Our main conclusions include the following: (1) the activation energy for electron transport and the phonon contribution to the heat conduction are nearly isotropic; (2) the thermal conductivity κ shows an enhancement at higher temperatures over classic phonon heat transfer. The anisotropic enhancement of κ is consistent with an EIM heat transfer along the c-axis chains; (3) strong spin-orbit $\lambda\mathbf{L}\cdot\mathbf{S}$ coupling within the trigonal-prismatic, high-spin Co2 sites leads to a strongly anisotropic magnetic susceptibility with a c-axis easy axis and a paramagnetic $\chi(T)$ that deviates from the Curie-Weiss law; (4) interchain antiferromagnetic coupling is frustrated; it transforms a ferromagnetic chain into a long-wavelength modulation with a possible spiral spin configuration. A small increase in the magnetization $M(H_\perp)$ relative to that in the paramagnetic phase at high magnetic fields supports the spiral spin configuration; and (5) the intrachain ferromagnetic coupling is caused by the indirect exchange interaction between a $\frac{3}{4}$-filled 1D band along the chain and a localized spin on the Co2 atoms. The presence of the helical exchange pathway introduced for interpreting the neutron results already violates the Ising model. Our findings [(2) and (4)] provide further evidence that the Ising model is not applicable in the magnetic insulator $Ca_3Co_2O_6$.

ACKNOWLEDGMENTS

We thank the Robert A. Welch Foundation and NSF (Grants No. DMR 0555663 and No. DMR0904282) for financial support.

*jszhou@mail.utexas.edu

[1] A. Maignan, C. Michel, A. C. Masset, C. Martin, and B. Raveau, Eur. Phys. J. B **15**, 657 (2000).
[2] N. Bellido, C. Simon, and A. Maignan, Phys. Rev. B **77**, 054430 (2008).
[3] H. Fjellvåg, E. Gulbrandsen, S. Aasland, A. Olsen, and B. C. Hauback, J. Solid State Chem. **124**, 190 (1996).
[4] E. V. Sampathkumaran, N. Fujiwara, S. Rayaprol, P. K. Madhu, and Y. Uwatoko, Phys. Rev. B **70**, 014437 (2004).
[5] S. Aasland, H. Fjellvåg, and B. Hauback, Solid State Commun. **101**, 187 (1997).
[6] T. Burnus, Z. Hu, M. W. Haverkort, J. C. Cezar, D. Flahaut, V. Hardy, A. Maignan, N. B. Brookes, A. Takana, H. H. Hsieh, H.-J. Lin, C. T. Chen, and L. H. Tjeng, Phys. Rev. B **74**, 245111 (2006).
[7] H. Wu, M. W. Haverkort, Z. Hu, D. I. Khomskii, and L. H. Tjeng, Phys. Rev. Lett. **95**, 186401 (2005).
[8] Y. B. Kudasov, Phys. Rev. Lett. **96**, 027212 (2006).
[9] S. Agrestini, L. C. Chapon, A. Daoud-Aladine, J. Schefer, A. Gukasov, C. Mazzoli, M. R. Lees, and O. A. Petrenko, Phys. Rev. Lett. **101**, 097207 (2008).
[10] A. V. Sologubenko, E. Felder, K. Giannó, H. R. Ott, A. Vietkine, and A. Revcolevschi, Phys. Rev. B **62**, R6108 (2000).
[11] A. V. Sologubenko, K. Giannó, H. R. Ott, A. Vietkine, and A. Revcolevschi, Phys. Rev. B **64**, 054412 (2001).
[12] A. V. Sologubenko, K. Giannó, H. R. Ott, U. Ammerahl, and A. Revcolevschi, Phys. Rev. Lett. **84**, 2714 (2000).
[13] K. Kordonis, A. V. Sologubenko, T. Lorenz, S.-W. Cheong, and A. Freimuth, Phys. Rev. Lett. **97**, 115901 (2006).
[14] A. V. Sologubenko, S. M. Kazakov, H. R. Ott, T. Asano, and Y. Ajiro, Phys. Rev. B **68**, 094432 (2003).
[15] D. L. Huber and J. S. Semura, Phys. Rev. **182**, 602 (1969).
[16] J. Rodriguez-Carvajal, Physica B **192**, 55 (1993).
[17] R. Berman, *Thermal Conduction in Solids* (Clarendon, Oxford, 1976).
[18] C. Hess and B. Büchner, Eur. Phys. J. B **38**, 37 (2004).
[19] V. Hardy, D. Flahaut, R. Frésard, and A. Maignan, J. Phys.: Condens. Matter **19**, 145229 (2007).
[20] S. S. P. Parkin and R. H. Friend, Philos. Mag. B **41**, 65 (1980).
[21] M. Drillon, L. Padel, and J.-C. Bernier, J. Chem. Soc., Faraday Trans. 1 **75**, 1193 (1979).
[22] H. Kageyama, K. Yoshimura, K. Kosuge, H. Mitamura, and T. Goto, J. Phys. Soc. Jpn. **66**, 1607 (1997).
[23] J. B. Goodenough, *Magnetism and the Chemical Bond* (Interscience, Wiley, New York, 1963).
[24] R. J. Elliott, *Magnetic Properties of Rare Earth Metals* (Plenum, New York, 1972).